Supporting Information

Xuexiang Huang[a,b,1], Xinyuan Ren[a,1], Yujun Cheng[a], Youhui Zhang[a], Zhe Sun[c], Sangjin Yang[c], Seoyoung Kim[c], Changduk Yang[c], Feiyan Wu[a] and Lie Chen[a,*]

[a] *College of Chemistry and Chemical Engineering / Institute of Polymers and Energy Chemistry (IPEC), Nanchang University, Nanchang 330031, Jiangxi, China.*

[b] *College of Intelligent Manufacturing and Materials Engineering, Gannan University of Science and Technology, 156 Kejia Avenue, Ganzhou 341000, Jiangxi, China.*

[c]*Department of Energy Engineering, School of Energy and Chemical Engineering, Perovtronics Research Center, Low Dimensional Carbon Materials Center, Ulsan National Institute of Science and Technology (UNIST), 50 UNIST-gil, Ulju-gun, Ulsan 44919, South Korea.*

[*]**Corresponding authors.**

Email addresses: chenlie@ncu.edu.cn (L. Chen)

[1] These authors contributed equally to this work.

1. Materials and Measurements

Materials: PCE10-2F were synthesized in our previous work, PCE10-2F has a molecular weight of 58.8 kDa, Y5, Y6, L8-BO and PM6 were purchased from Derthon Optoelectronic Materials Science Technology Co LTD (Shenzhen, China). All reagents and commercially available compounds are used upon receipt.

Measurements

Optical absorption spectra of the polymers were measured on a PerkinElmer model Lambda 900 UV-vis/near-IR spectrophotometer. Solution and solid-state absorption spectra were obtained from dilute (10^{-6} M) polymer solution in chloroform and from thin films on glass substrate, respectively. Thin films were spin coated from 20 mg/mL solutions in chloroform.

The specimen for atomic force microscopy (AFM) measurements was prepared using the same procedures those for fabricating devices but without PDINO/Ag on top of the active layer. Transmission electron microscope (TEM) images were taken on a JEOL-2100F transmission electron microscope and an internal charge-coupled device (CCD) camera. The specimen for TEM measurement was prepared by spin casting the blend solution on ITO/PEDOT: PSS substrate, then floating the film on a water surface, and transferring to TEM grids.

The GIWAXS measurement was carried out at the PLS-II 6A U-SAXS beamline of the Pohang Accelerator Laboratory in Korea. The X-rays coming from the in-vacuum undulator (IVU) were monochromated (wavelength λ = 1.10994 Å) using a double crystal monochromator and focused both horizontally and vertically (450 (H) x 60 (V) um^2 in FWHM @ the sample position) using K-B type mirrors. The grazing incidence wide-angle X-ray scattering (GIWAXS) sample stage was equipped with a 7-axis motorized stage for the fine alignment of the sample, and the incidence angles of the X-ray beam were set to be 0.11°-0.13° for the neat and blend films. The GIWAXS patterns were recorded with a 2D CCD detector (Rayonix SX165) and an X-ray irradiation time within 100 s, dependent on the saturation level of the detector. Diffraction angles were calibrated using a sucrose standard (monoclinic, P21, a=10.8631Å, b =8.7044Å, c=7.7624Å, and b=102.938Å) and the sample-to-detector distance was ~231 mm.

Solar cell characterization: The current density-voltage (*J-V*) curves of OSCs were measured in the glovebox with Keithley 2400, under AM 1.5G illumination at 100 mW cm^{-2} irradiation using an Enli SS-F5-3A solar simulator, and the light intensity was calibrated with a standard Si solar cell with KG2 filter (made by Enli Technology Co., Ltd., Taiwan, and calibrated report can be traced to NREL). The EQE spectrum was measured using a QE-R Solar Cell Spectral Response Measurement System (Enli Technology Co., Ltd.,Taiwan).

2. Device fabrication

2.1 Opaque device fabrication

The device is fabricated with ITO/PEDOT:PSS/active layer/PDINO/Ag tradition structure. The ITO coated glass substrates were cleaned by ultrasound for 15 minutes in sequence in water/detergent, water, acetone and isopropanol, and then treated in ultraviolet-ozone for 1400 seconds. The PEDOT:PSS solution was spin-coated on top of the cleaned ITO-coated glass substrate and the PEDOT:PSS film thickness was approximately 25 nm. After annealing at 150 °C for 20 min, then the substrates were transferred into a glove box. For the solar cells based on NBG system, PCE10-2F or (PCE10-2F+DA, 1:0.2) with a concentration of 8 mg mL^{-1} in CF were spun onto the PEDOT: PSS layers at 2500 rpm (60 nm) for 40 s form the front layer, Y6 and (Y6:Y5, 1:0.1) with a concentration of 10 mg mL^{-1} in CF, and 1,8-diiodooctane (DIO) and CN was added (volume ratio 0.25% and 0.25%, respectively). then spun onto the PCE10-2F layers at 2300 rpm (40nm) for 40 s. After annealing at 100 °C for 10 min. For the solar cells based on WBG system, The PM6: acceptors active layers (D:A = 1:1.2) weight ratio for binary, The DA:PM6: L8-BO:Y5 active layers (D:A = 0.25:1:1.1:0.1) weight ratio for quaternary, were then spin-coated from 16.5 mg/mL chloroform solution with 0.3 vol.% 1,8-diiodooctane (DIO) for PM6:L8-BO binary blend and DA:PM6: L8-BO:Y5 quaternary active layers, at 3000 rpm for the 30s to form an active layer of around 100 nm. The PDINO was dissolved in methanol at 3 mg mL^{-1} and spin-coated on active layer at 3000 rpm for 30s. Finally, 90-nanometer thick Ag layers were deposited on the active layer under high vacuum of ~$3x10^{-4}$Pa. The overlapping area of cathode and anode was 4 square millimeters. J-V curves of devices based on polymer doner: Y6 were measured under the standard AM 1.5G spectrum of 100 MW cm^{-2}. **Semitransparent device fabrication** was fabricated by following the same procedure. 15nm or 25nm thickness Ag and layers were deposited on the active layer under high vacuum of ~$3x10^{-4}$Pa. Then, MoO_3 (35 nm) were evaporated onto the surface of Ag. The overlapping area of cathode and anode was 4 square millimeters. J-V curves of ST-OSC devices were measured under the standard AM 1.5G spectrum of 100 MW cm^{-2}.

Electroluminescence (EL) quantum efficiency (EQE_{EL}) measurements were performed by applying external voltage sources through the devices from 1V to 4V. A

Keithley 2400 SourceMeter was used for supplying voltages and recording injected current, and a Keithley 485 picoammeter was used for measuring the emitted light intensity.

3. Optical Characterization

The average visible transmittance (AVT) is calculated using

$$VLT = \frac{\int T(\lambda)P(\lambda)S(\lambda)d(\lambda)}{\int P(\lambda)S(\lambda)d(\lambda)} VLT = \frac{\int T(\lambda)P(\lambda)S(\lambda)d(\lambda)}{\int P(\lambda)S(\lambda)d(\lambda)}$$

$$AVT = \frac{\int T(\lambda)V(\lambda)S(\lambda)d(\lambda)}{\int P(\lambda)S(\lambda)d(\lambda)} \quad \text{(Eq. S1)}$$

where λ is the wavelength, T is the transmission, V is the normalized photopic spectral response of the eye, and S is the solar photon flux (AM1.5G). It is estimated by taking the average of the transparency of the devices in the visible region (380-740 nm) based on the photonic response of the human eye.

Infrared photon rejection rate (IRR) is defined as:

$$\text{IRR} = 1 - \frac{\int T(\lambda)S(\lambda)d\lambda}{\int S(\lambda)d\lambda}$$

where T is the transmittance, S is the solar photon flux, and λ is the wavelength.

All the photographs are taken by Apple iPhone13 Pro.

4. Thermal Insulation Performance Test

The model of the infrared heater is Philips PAR38E, the power is 150W, and the irradiation distance is 25cm.

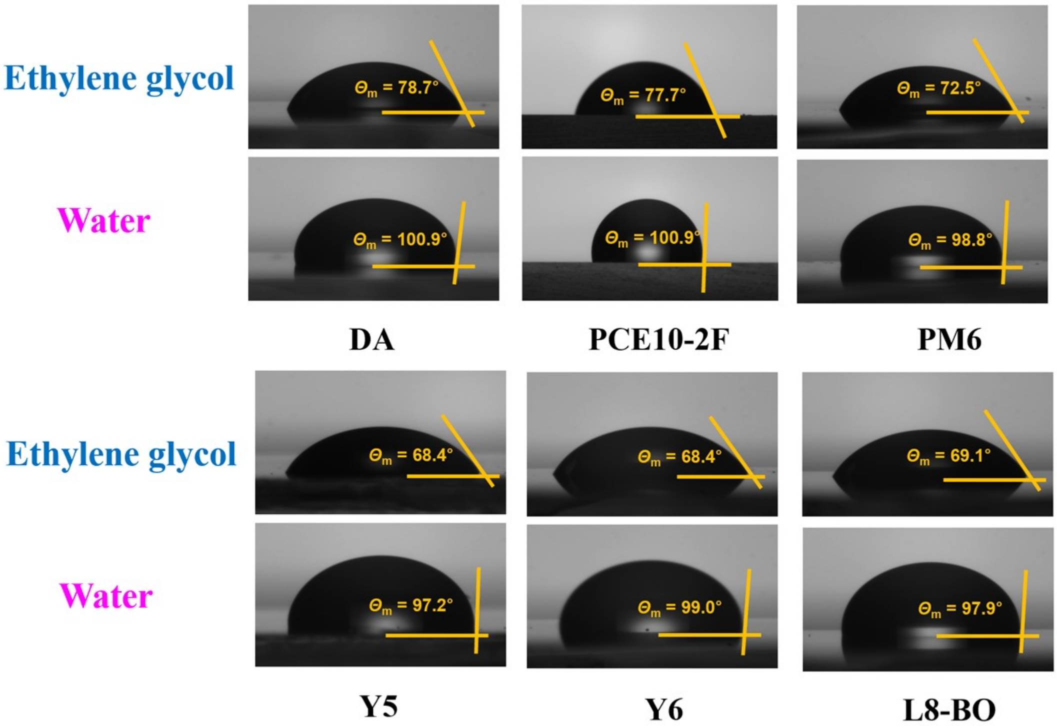

Figure S1. Contact angle images of DA, PCE10-2F, PM6, Y5, Y6 and L8-BO films with water and ethylene glycol droplet on top.

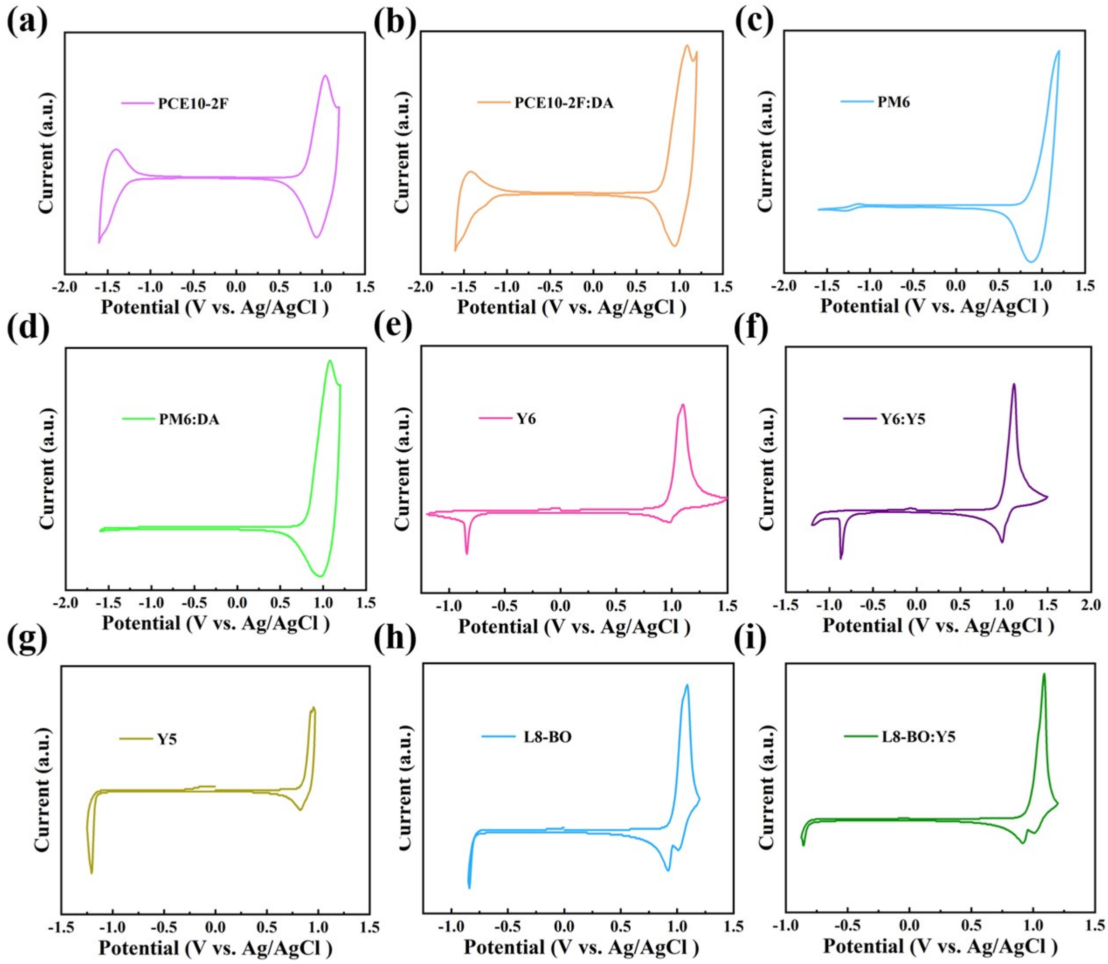

Figure S2. (a-i) CV curves of PCE10-2F, PCE10-2F:DA, PM6, PM6:DA, Y6, Y5, Y6:Y5, L8-BO and L8-BO:Y5 blend films.

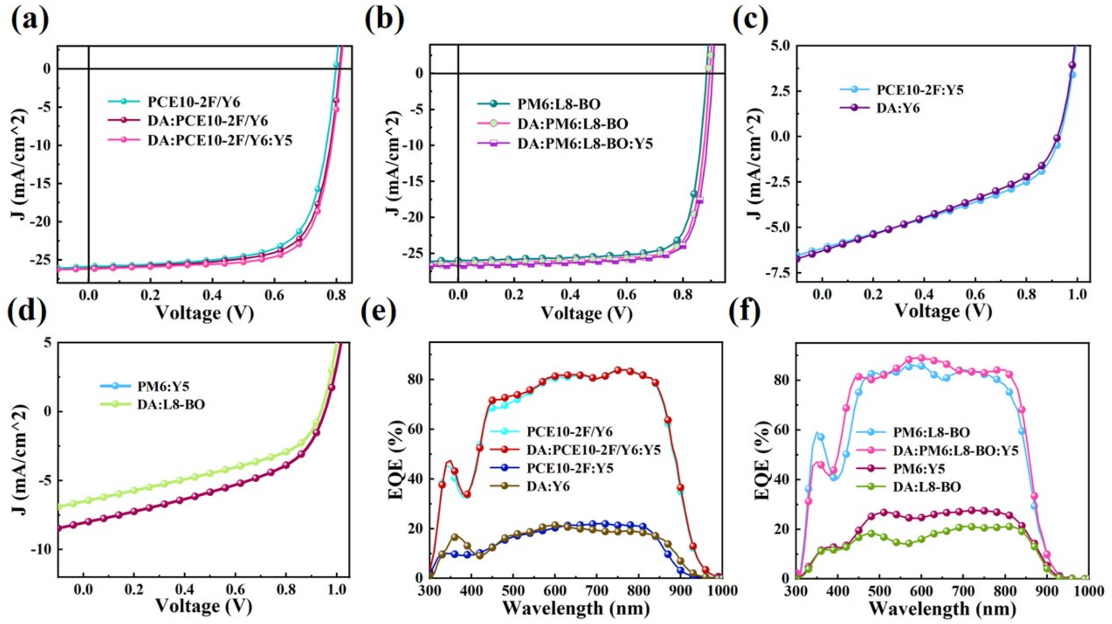

Figure S3. (a) J-V curves of PCE10-2F/Y6, DA: PCE10-2F/Y6 and DA: PCE10-2F/Y6:Y5-based OSC devices. (b) J-V curves of PM6:L8-BO, DA PM6:L8-BO and DA: PM6:L8-BO:Y5-based OSC devices. (c) J-V curves of PCE10-2F:Y5, DA:Y6-based OSC devices. (d) J-V curves of PM6:Y5, DA:L8-BO-based OSC devices. (e) EQE curves of PCE10-2F/Y6, DA: PCE10-2F/Y6:Y5, PCE10-2F:Y5 and DA:Y6-based OSC devices. (f) EQE curves of PM6:L8-BO, DA: PM6:L8-BO:Y5, PM6:Y5 and DA:L8-BO -based OSC devices.

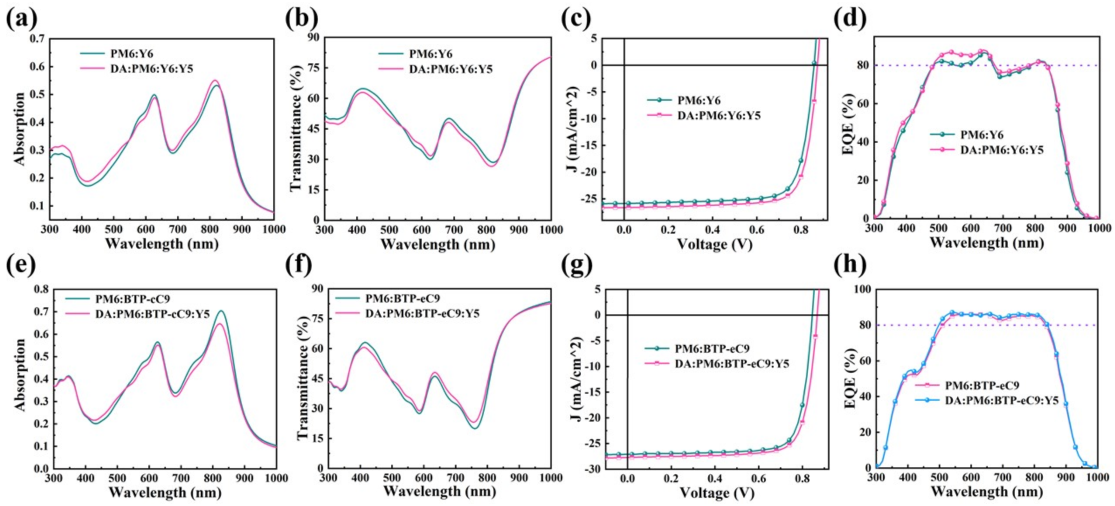

Figure S4. (a) Absorption spectra and (b) transmittance spectra of PM6:Y6, DA: PM6:Y6:Y5 blend films. (c) *J-V* and (d) EQE curves of PM6:Y6 and DA:PM6:Y6:Y5-based OSC devices. (e) Absorption spectra and (f) transmittance spectra of PM6:BTP-eC9, DA:PM6:BTP-eC9:Y5 blend films. (g) *J-V* and (h) EQE curves of PM6:BTP-eC9, DA:PM6:BTP-eC9:Y5-based OSC devices.

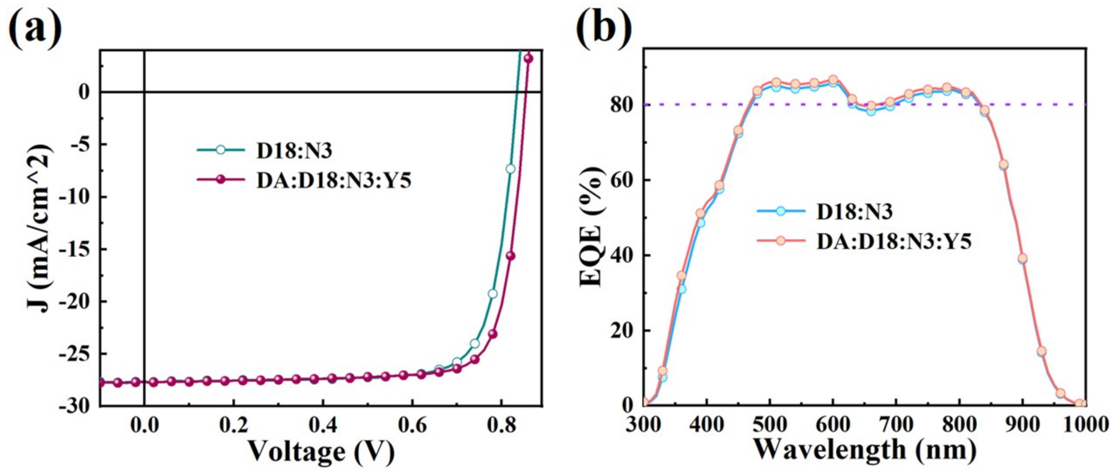

Figure S5. (a) *J-V* and (b) EQE curves of D18/N3, DA: D18/N3:Y5-based OSC devices.

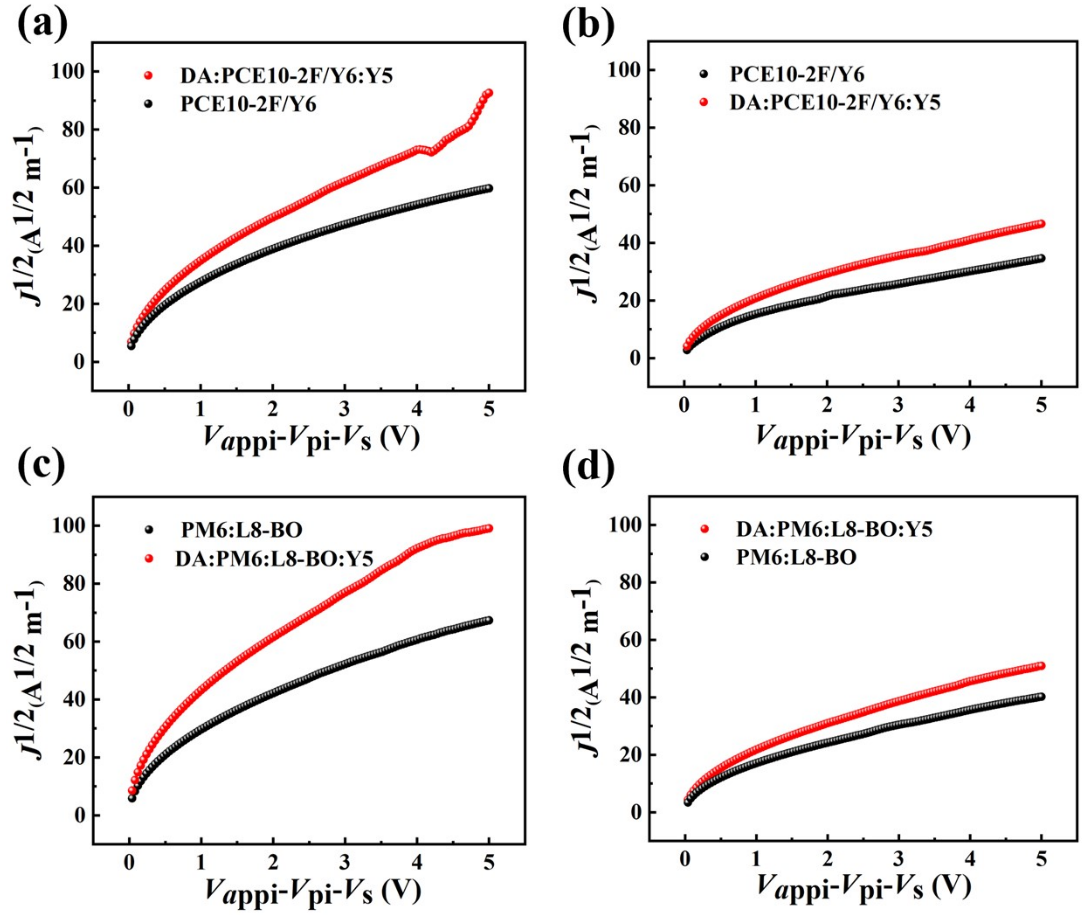

Figure S6. $J^{1/2}$−V plots of hole-only devices and $J^{1/2}$−V plots of electron-only devices (in dark).

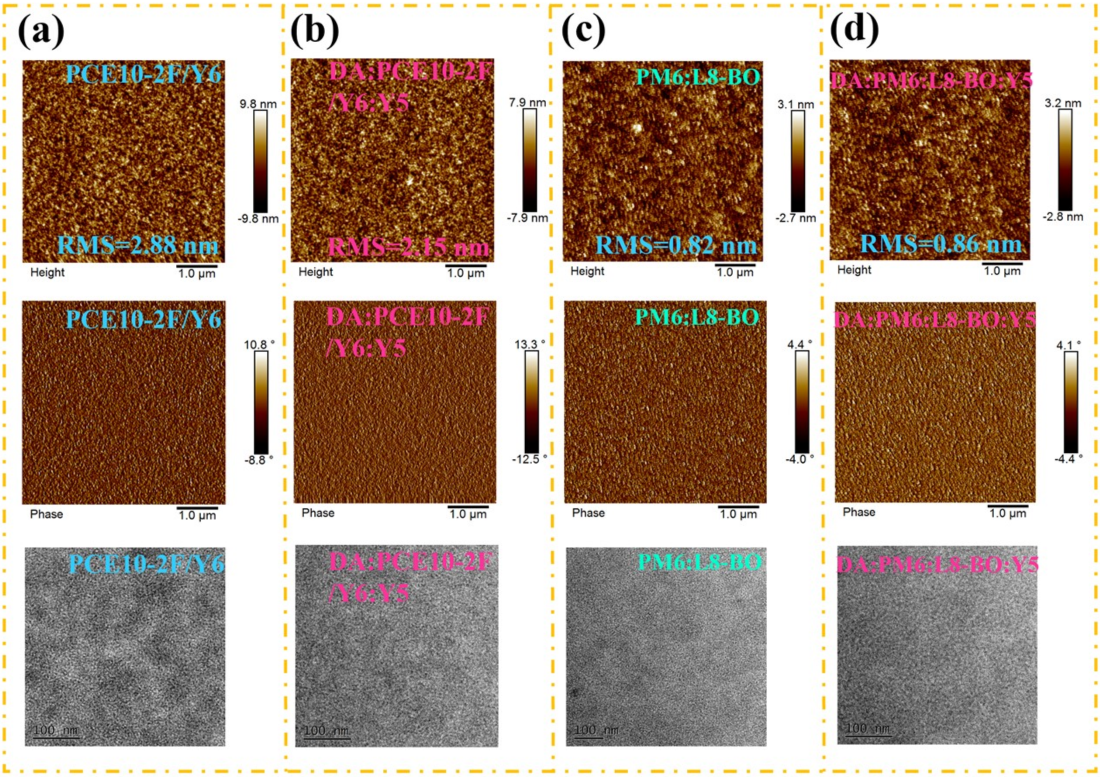

Figure S7. AFM and TEM images of optimized WBG system blend films.

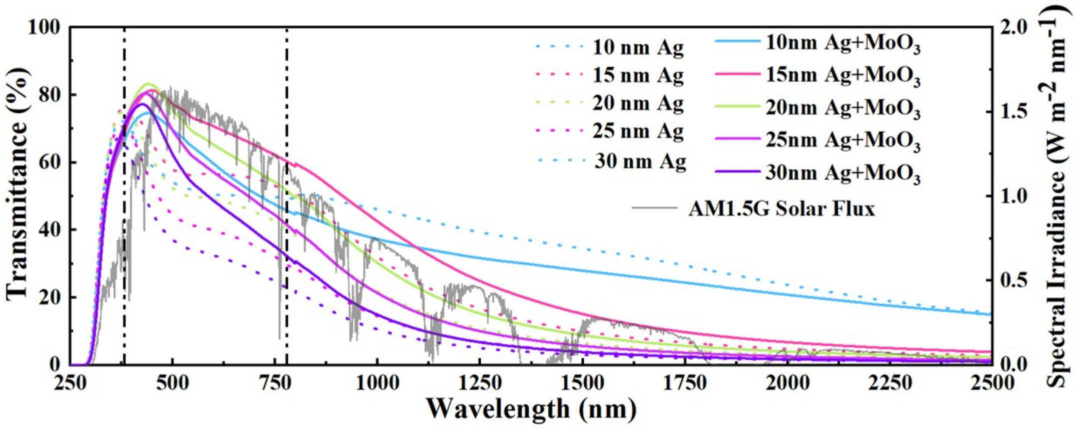

Figure S8. (a) Transmittance of 10 nm, 15 nm, 20 nm, 25 nm, 30 nm Ag thickness back electrode (ITO/Glass/PDINN/Ag/with or without MoO_3).

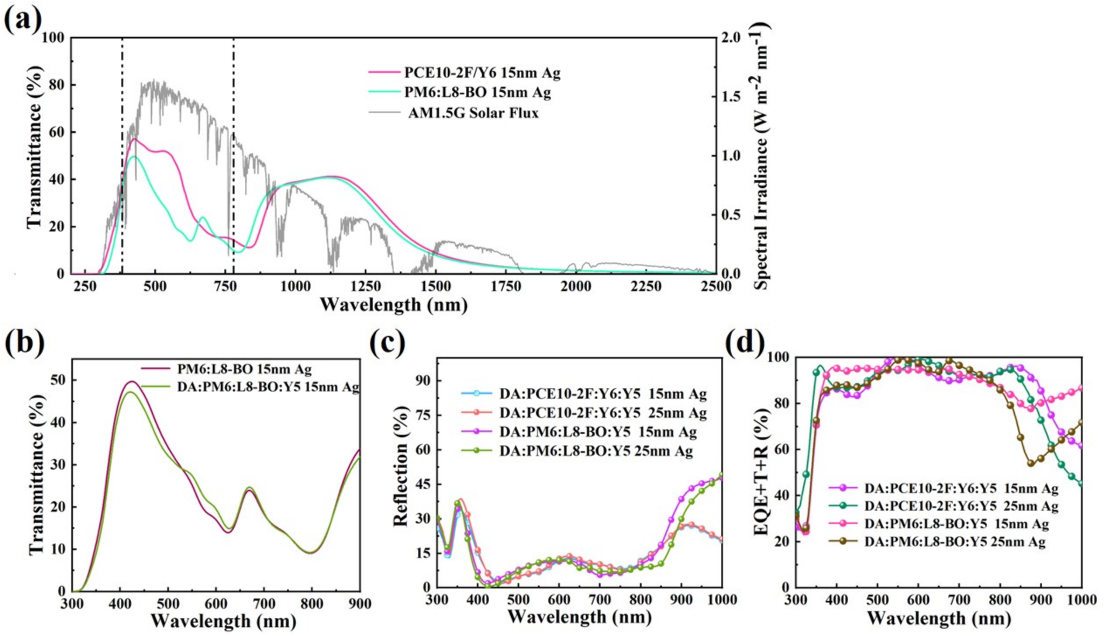

Figure S9. (a-b) Transmittance spectra of PCE10-2F/Y6, PM6:L8-BO and DA:PM6:L8-BO:Y5-based ST-OSCs. (c-d) The reflectance spectra and photon balance check spectra (EQE(λ)%+T(λ)%+R(λ)%) spectra of ST-OSCs.

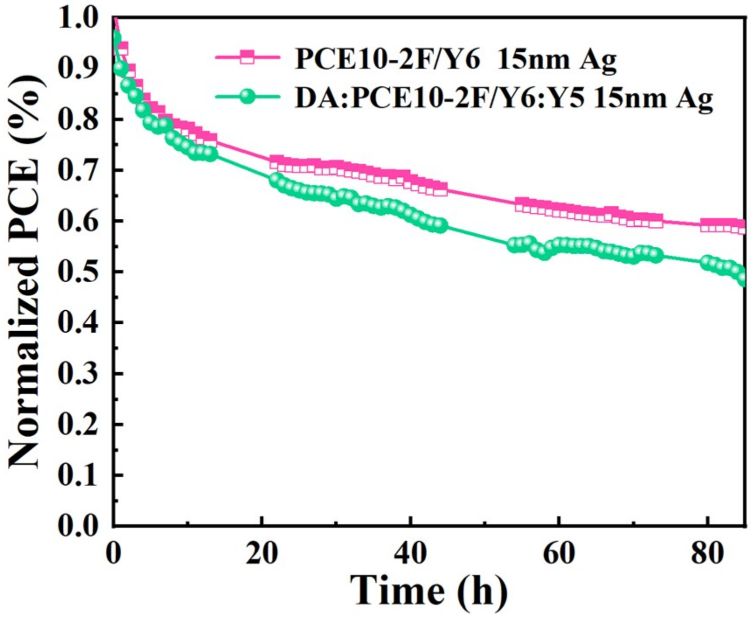

Figure S10. Stability of ST-OSCs under AM 1.5G 100 mW cm^{-2} simulated sunlight continuous illumination with 1h intervals for data collection.

Table S1. Photovoltaic performance of binary and multi-component OSCs with different DA and Y5 ratio.

Device	D/A	V_{OC} (V)	J_{SC} (mA/ cm^2)	FF (%)	PCE (%)
PCE10-2F/Y6	60/40nm	0.796	25.87	70.56	14.55
PCE10-2F/Y5	60/40nm	0.930	6.14	38.20	2.17
DA/Y6	60/40nm	0.921	6.28	35.62	2.05
DA:PCE10-2F/Y6	0.1:1, 60/40nm	0.801	25.92	70.70	14.68
	0.2:1, 60/40nm	0.808	26.13	71.40	15.11
	0.3:1, 60/40nm	0.811	25.77	69.23	14.47
PCE10-2F/Y6:Y5	60/40nm, 1:0.1	0.803	26.04	70.98	14.84
DA:PCE10-2F/Y6:Y5	0.2:1,60/40nm,1:0.05	0.808	25.99	73.88	15.51
	0.2:1,60/40nm, 1:0.1	0.812	26.20	73.22	15.57
	0.2:1,60/40nm, 1:0.15	0.816	25.37	70.42	14.58
PM6:L8-BO	1:1.2	0.880	25.96	78.79	18.01
PM6:Y5	1:1.2	0.952	8.05	42.76	3.27
DA:L8-BO	1:1.2	0.937	6.51	40.54	2.46
DA:PM6:L8-BO	0.15:1:1.2	0.888	26.14	79.89	18.54
	0.25:1:1.2	0.892	26.44	79.41	18.74
	0.35:1:1.2	0.895	25.79	78.34	18.08
PM6:L8-BO:Y5	1:1.2:0.1	0.888	26.11	79.08	18.34
DA:PM6:L8-BO:Y5	0.25:1:1.2:0.1	0.903	26.69	79.18	19.09

Table S2. Operating characteristics of opaque devices under simulated AM 1.5G, 100 mW cm^{-2} illumination.

Devices	D/A	V_{OC} (V)	J_{SC} (mA/cm^2)	$J_{SC\ cal}$[(a)] (mA/cm^2)	FF (%)	PCE [(b)] (%)	AVT of active layer (%)
PM6:Y6	1:1.2	0.859	25.86	25.09	77.05	17.12(16.93)	38.84
DA: PM6:Y6:Y5	0.25:1:1.2:0.1	0.874	26.63	25.84	77.62	18.08(17.79)	40.40
PM6:BTP-eC9	1:1.2	0.843	27.11	26.20	78.74	18.00(17.83)	36.11
DA: PM6:BTP-eC9:Y5	0.25:1:1.2:0.1	0.865	27.71	26.59	78.11	18.72(18.59)	37.82
D18:N3	60 nm/45 nm	0.832	27.66	26.37	78.14	17.98(17.69)	35.23
DA:D18:N3:Y5	0.2:1,60nm/1:0.1,45nm	0.853	27.70	26.45	79.67	18.80(18.66)	36.07

Table S3. Hole and electron mobilities of PCE10-2F/Y6, DA:PCE10-2F/Y6:Y5, PM6:L8-BO and DA:PM6:L8-BO:Y5 devices in the dark.

Device	μ_h (cm^2 V^{-1} s^{-1})	μ_e (cm^2 V^{-1} s^{-1})	μ_h/μ_e
PCE10-2F/Y6	8.685×10^{-4}	8.155×10^{-4}	1.064
DA:PCE10-2F/Y6:Y5	9.008×10^{-4}	8.805×10^{-4}	1.023
PM6:L8-BO	8.945×10^{-4}	8.559×10^{-4}	1.045
DA:PM6:L8-BO:Y5	9.145×10^{-4}	8.948×10^{-4}	1.022

Table S4. Summarized parameters for the ordering structures of neat films and blend films.

Film	Out-of-Plane				In-Plane			
	π-π stacking cell axis (010)				Unit cell long axis (100)			
	q ($Å^{-1}$)	d-spacing (Å)	FWHM ($Å^{-1}$)	Coherence length (Å)	q ($Å^{-1}$)	d-spacing (Å)	FWHM ($Å^{-1}$)	Coherence length (Å)
PCE10-2F	1.606	3.910	0.278	20.5	0.262	24	0.1	56.3
PCE10-2F:DA	1.631	3.850	0.43	23.5	0.270	23.3	0.083	68.5
Y6	1.731	3.627	0.155	36.8	0.273	23	0.07	80.8
Y6:Y5	1.738	3.613	0.176	32.5	0.276	22.7	0.082	69.4
PCE10-2F/Y6	1.691	3.714	0.144	39.8	0.298	21.1	0.041	136.8
DA:PCE10-2F/Y6:Y5	1.637	3.562	0.250	22.9	0.301	20.9	0.057	70.4
PM6	1.653	3.799	0.294	19.4	0.285	22.0	0.089	63.3
PM6:DA	1.721	3.649	0.187	30.6	0.299	21	0.054	104.4
PM6:L8-BO	1.702	3.690	0.164	34.8	0.270	23.3	0.066	85.6
DA:PM6:L8-BO:Y5	1.713	3.666	0.188	30.4	0.272	23.1	0.069	82.5

Table S5. Detailed parameters of silver electrodes with different thickness.

Electrode	AVT (%)	IRR (%)	Sheet resistance (Ω)
100nm Ag	0	100	1.58
10nm Ag	63.66	65.22	6.89
15nm Ag	73.16	64.62	2.74
20nm Ag	69.10	73.78	2.50
25nm Ag	61.71	80.81	2.32
30nm Ag	53.77	86.10	1.96

Table S6. Detailed parameter on state-of-the-art ST-OSC devices without complex optical engineering reported in the literatures.

Acytive layer	PCE (%)	AVT (%)	LUE (%)	Reference
DA:PCE10-2F/Y6:Y5	12.95	31.35	4.06	This work
DA:PCE10-2F/Y6:Y5	11.18	45.61	5.10	This work
DA:PM6:L8-BO:Y5	13.56	25.08	3.44	This work
PM6:BTP-eC9:L8-BO	11.44	46.79	5.35	1
PCE-10:A078	10.8	45.7	5.0	2
PBDB-TF:L8-BO:BTP-eC9	12.95	38.67	5.0	3
PTB7-Th: H3	8.38	50.9	4.27	4
PTB7-Th: FOIC: $PC_{71}BM$	8.66	50.04	4.33	5
PL-Cl: F8IC	11.0	35.0	3.85	6
PTB7-Th: FOIC	10.3	37.4	3.85	7
PBT1-C-2Cl: Y6	9.1	40.1	3.65	8
PCE-10: BT-CIC: TT-FIC	8.0	44.2	3.54	9
PTB7-Th: IEICO-4Cl	8.38	25.7	2.15	10
PTB7-Th: IUIC	10.2	31	3.16	11
PCE-10: BT-CIC	7.1	43	3.05	12
PTB7-Th: ATT-2	7.7	37	2.85	13
PBDB-T: ITIC	7.3	25.2	1.84	14
PTB7-Th: IHIC	9.77	36	3.52	15
PTB7-Th: COi8DFIC: IEICO-4F	8.23	20.78	1.71	16

PBDTTT-ET: IEICO	6.8	25.1	1.71	17
PTB7-Th: PBT1-S: PC71BM	9.2	20	1.84	18
PBDB-T-2F: Y6	12.88	25.6	3.30	19
PTB7-Th: ACS8	11.1	28.6	3.17	20
PTB7-Th: BDTThIT-4F: IEICO-4F	9.40	24.6	2.31	21
PTB7-Th: IEICO-4F	9.06	27.1	2.46	22
PTB7-Th: IEICO-4F	10.03	34.2	3.43	23
PBDB-T: Y14	12.67	23.69	3.00	24
PBFTT: IT-4Cl	9.1	27.6	2.51	25
PFTzTT3TC: ITIC	6.43	26.77	1.72	26
PBN-S: IT-4F	9.83	32	3.15	27
PTB7-Th: IEICO-4F	10.83	29.5	3.19	28
PDTP-DFBT: FOIC	4.2	52	2.18	29
J71:PTB7-Th: IHIC	9.3	21.4	2.01	30
DTG-IW: PTB7-Th	6.19	50.4	3.12	31
PM6: Y6: PC71BM	10.2	28.6	2.92	32
PBDB-TF: Y6: BTTPC	13.1	22.35	2.93	33
PBDB-TF: Y6: DTNIF	13.49	22.58	3.05	34
PBDB-TF: Y6: PC71BM	13	21.4	2.78	35
PCE10: ICBA:Y8	10.46	26.56	2.78	36
D18-Cl: Y6-1O: Y6	13.02	20.2	2.63	37

PCE10-2Cl: IT-4F	8.25	33	2.72	38
PM2: Y6-BO	5.9	43.3	2.55	39
PM6: Y6: DIBC	14.00	21.60	3.02	40
PM6: Y6	9.7	42.82	4.15	41
PCE10-BDT2F-0.8: Y6	10.85	41.08	4.46	42
PTB7-Th: ATT-9	9.37	35.5	3.33	43
PM6-Ir1: BTP-eC9: PC71BM	14.09	20.44	2.82	44

Table S7. Detailed parameter on state-of-the-art multifunctional ST-OSC devices reported in the literatures.

Device structure	PCE (%)	AVT (%)	LUE (%)	IRR (%)	Reference
ITO/PEDOT:PSS/active layer/PDINN/ Ag /MoO3	12.83	31.35	4.02	90	45
ITO/PEDOT:PSS-TA/active layer/Bis-FIMG/ultrathin Ag /DBR	11.18	32.07	3.58	90	46
ITO/PEDOT:PSS/active layer/PDINN/Ag	9.37	35.5	3.33	84.3	47
ITO/PEDOT:PSS/active layer/PFN-Br/Ag /DBR	12.3	23.45	2.88	90	48
ITO/PEDOT:PSS/active layer/PFN-Br/Ag /DBR	8.4	22.8	1.92	83.1	49
ITO/PEDOT:PSS/active layer/PFN-Br/Ag /DBR	7.3	29.5	2.15	93.1	55

REFERENCES

[1] X. Liu, Z. Zhong, R. Zhu, J. Yu and G. Li, *Joule*, 2022, **6**, 1–13.

[2] Y. Li, X. Guo, Z. Peng, B. Qu, H. Yan, H. Ade, M. Zhang and S. R. Forrest, *P.N.A.S.* 2020, **117**, 21147.

[3] S. Guan, Y. Li, K. Yan, W. Fu, L. Zuo and H. Chen, *Adv. Mater.*,

https://doi.org/10.1002/adma.202205844.

[4] Y. Li, C. He, L. Zuo, F. Zhao, L. Zhan, X. Li, R. Xia, H.L. Yip, Li, C.Z., X. Liu, and H. Chen, *Adv. Energy Mater*., 2021,**11**, 2003408.

W. Li, M. Chen, J. Cai, E. L.K. Spooner, H. Zhang, R. S. Gurney, D. Liu, Z. Xiao, D. G. Lidzey, L. Ding and T. Wang, *Joule*, 2019, **3**, 819-833.

[5] Q. Liu, L.G. Gerling, F. Bernal-Texca, J. Toudert, T. Li, X. Zhan, and J. Martorell, *Adv. Energy Mater*., 2020, **10**, 1904196.

[6] Y. Chang, X. Zhu, L. Zhu, Y. Wang, C. Yang, X. Gu, Y. Zhang, J. Zhang, K. Lu, X. Sun and Z. Wei, *Nano Energy*, 2021, **86**, 106098.

[7] T. Li, S. Dai, Z. Ke, L. Yang, J. Wang, C. Yan, W. Ma, and X. Zhan, *Adv. Mater*. 2018, **30**, 1705969.

[8] Y. Xie, Y. Cai, L. Zhu, R. Xia, L. Ye, X. Feng, H.L. Yip, F. Liu, G. Lu, S. Tan, and Y. Sun, *Adv. Funct. Mater*., 2020, **30**, 2002181.

[9] Y. Li, C. Ji, Y. Qu, X. Huang, S. Hou, C.Z. Li, L.S. Liao, L.J. Guo and S.R. Forrest, *Adv. Mater*., 2019, **31**, 1903173.

[10] Y. Cui, C. Yang, H. Yao, J. Zhu, Y. Wang, G. Jia, F. Gao and J. Hou, *Adv. Mater*., 2017, **29**, 1703080. 2.

[11] B. Jia, S. Dai, Z. Ke, C. Yan, W. Ma and X. Zhan, *Chem. Mater*., 2017, **30**, 239-245.

[12] Y. Li, J.D. Lin, X. Che, Y. Qu, F. Liu, L.S. Liao and S.R. Forrest, *J. Am. Chem. Soc*., 2017, **139**, 17114-17119.

[13] F. Liu, Z. Zhou, C. Zhang, J. Zhang, Q. Hu, T. Vergote, F. Liu, T.P. Russell, and

X. Zhu, *Adv. Mater.*, 2017, **29**, 1606574.

[14] M.B. Upama, M. Wright, N.K. Elumalai, M.A. Mahmud, D. Wang, C. Xu and A. Uddin, *ACS Photonics,* 2017, **4**, 2327-2334.

[15] W. Wang, C. Yan, T.K. Lau, J. Wang, K. Liu, Y. Fan, X. Lu and X. Zhan, *Adv. Mater.,* 2017, **29**, 1701308.

[16] X. Ma, Z. Xiao, Q. An, M. Zhang, Z. Hu, J. Wang, L. Ding and F. Zhang, *J. Mater. Chem. A,* 2018, **6**, 21485-21492.

[17] C. Sun, R. Xia, H. Shi, H. Yao, X. Liu, J. Hou, F. Huang, H.-L. Yip and Y. Cao, *Joule,* 2018, **2**, 1816-1826.

[18] Y. Xie, L. Huo, B. Fan, H. Fu, Y. Cai, L. Zhang, Z. Li, Y. Wang, W. Ma, Y. Chen,and Y. Sun, *Adv. Funct. Mater*. 2018, **28**, 1800627.

[19] X. Song, N. Gasparini, L. Ye, H. Yao, J. Hou, H. Ade and D. Baran, *ACS Energy Lett.*, 2018, **3**, 669-676.

[20] J. Wang, J. Zhang, Y. Xiao, T. Xiao, R. Zhu, C. Yan, Y. Fu, G. Lu, X. Lu, S. R. Marder and X. Zhan, *J. A. C. S.*, 2018, **140**, 9140-9147.

[21] Y. Bai, C. Zhao, X. Chen, S. Zhang, S. Zhang, T. Hayat, A. Alsaedi, Z.a. Tan, J. Hou and Y. Li, *J. Mater. Chem. A,* 2019, **7**, 15887-15894.

[22] Z. Hu, Z. Wang and F. Zhang, *J. Mater. Chem. A,* 2019, **7**, 7025-7032.

[23] Y. Liu, P. Cheng, T. Li, R. Wang, Y. Li, S.Y. Chang, Y. Zhu, H.W. Cheng, K.H. Wei, X. Zhan, B. Sun and Y. Yang, *ACS Nano*, 2019,**13**, 1071-1077.

[24] M. Luo, C. Zhao, J. Yuan, J. Hai, F. Cai, Y. Hu, H. Peng, Y. Bai, Z.a. Tan and Y. Zou, *Mater. Chem. Front*., 2019, **3**, 2483-2490.

[25] W. Su, Q. Fan, X. Guo, J. Wu, M. Zhang and Y. Li, *Phys. Chem. Chem. Phys.*, 2019, **21**, 10660-10666.

[26] X. Wang, K. Zhu, X. Jing, Q. Wang, F. Li, L. Yu and M. Sun, *ACS Appl. Energy Mater*, 2019, **3**, 915-922.

[27] Y. Wu, H. Yang, Y. Zou, Y. Dong, J. Yuan, C. Cui and Y. Li, *Energy Environ. Sci.*, 2019, **12**, 675-683.

[28] R. Xia, C.J. Brabec, H.-L. Yip and Y. Cao, *Joule,* 2019, **3**, 2241-2254.

[29] Y. Xie, R. Xia, T. Li, L. Ye, X. Zhan, H.L. Yip and Y. Sun, *Small Methods*, 2019, **3**, 1900424.

[30] J. Zhang, G. Xu, F. Tao, G. Zeng, M. Zhang, Y.M. Yang, Y. Li and Y. Li, *Adv. Mater*. 2019, **31**, 1807159.

[31] Y. Cho, T.H. Lee, S. Jeong, S.Y. Park, B. Lee, J.Y. Kim and C. Yang, *ACS Appl. Energy Mater*. 2020, **3**, 7689-7698.

[32] B.H. Jiang, H.E. Lee, J.H. Lu, T.H. Tsai, T.S. Shieh, R.J. Jeng and C.P. Chen, *ACS Appl. Mater. Interfaces*, 2020, **12**, 39496-39504.

[33] D. Wang, R. Qin, G. Zhou, X. Li, R. Xia, Y. Li, L. Zhan, H. Zhu, X. Lu, H.L. Yip, H. Chen, C. Li, *Adv. Mater.*, 2020, **32**, 2001621.

[34] P. Yin, Z. Yin, Y. Ma and Q. Zheng, *Energy Environ. Sci.*, 2020, **13**, 5177-5185.

[35] N. Zhang, T. Jiang, C. Guo, L. Qiao, Q. Ji, L. Yin, L. Yu, P. Murto and X. Xu, *Nano Energy,* 2020, **77**, 105111.

[36] C. Zhu, H. Huang, Z. Jia, F. Cai, J. Li, J. Yuan, L. Meng, H. Peng, Z. Zhang, Y. Zou, and Y Li., *Sol Energy,* 2020, **204**, 660-666.

[37] Z. Hu, J. Wang, X. Ma, J. Gao, C. Xu, X. Wang, X. Zhang, Z. Wang and F. Zhang, *J. Mater. Chem. A*, 2021, **9**, 6797-6804.

[38] X. Huang, J. Oh, Y. Cheng, B. Huang, S. Ding, Q. He, F. Wu, C. Yang, L. Chen and Y. Chen, *J. Mater. Chem*. A, 2021, **9**, 5711-5719.

[39] T. Jiang, G. Zhang, R. Xia, J. Huang, X. Li, M. Wang, H.-L. Yip and Y. Cao, *Mater. Today Energy*, 2021, **21**, 100807.

[40] X. Lu, L. Cao, X. Du, H. Lin, C. Zheng, Z. Chen, B. Sun and S. Tao, *Adv. Opt. Mater*., 2021, **9**, 2100064.

[41] H.I. Jeong, S. Biswas, S.C. Yoon, S.J. Ko, H. Kim and H. Choi, *Adv. Energy Mater*., 2021, **11**, 2102397

[42] X. Huang, L. Zhang, Y. Cheng, J. Oh, C. Li, B. Huang, L. Zhao, J. Deng, Y. Zhang, Z. Liu, F. Wu, X. Hu, C. Yang, L. Chen, Y. Chen, *Adv. Funct. Mater*. 2022, **32**, 2108634.

[43] W. Liu, S. Sun, S. Xu, H. Zhang, Y. Zheng, Z. Wei and X. Zhu *Adv. Mater*., 2022, **18**, 2200337.

[44] W. Liu, S. Sun, S. Xu, H. Zhang, Y. Zheng, Z. Wei, and X. Zhu, *Adv. Mater*., 2022, **34**, 2200337.

[45] D. Wang, R. Qin, G. Zhou, X. Li, R. Xia, Y. Li, L. Zhan, H. Zhu, X. Lu, H. Yip, H. Chen and C. Li, *Adv. Mater*. **2020**, 32, 2001621.

[46] W. Liu, S. Sun, S. Xu, H. Zhang, Y. Zheng, Z. Wei and X. Zhu *Adv. Mater*., 2022, **18**, 2200337.

[47] C. Sun, R. Xia, H. Shi, H. Yao, X. Liu, J. Hou, F. Huang, H. Yip and Y. Cao.

Joule, 2018, **2**, 1816-1826.

[48] D. Wang, Y. Li, G. Zhou, E. Gu, R. Xia, B. Yan, J. Yao, H. Zhu, X. Lu, H. Yip, H. Chen and C. Li, *Energy Environ. Sci*., 2022, **15**, 2629-2637.

[49] X. Lia, R. Xia, K. Yan, H. Yip, H. Chen, C. Li. *Chinese Chem. Lett*., 2020, **31**, 1608-1611.